TECHNICAL PAPER

Modeling, performance simulation and controller design for a hybrid fuel cell electric vehicle

A. Yazdani · A. H. Shamekhi · S. M. Hosseini

Abstract In this paper, a PEM fuel cell hybrid vehicle performance is studied. Main components of this hybrid vehicle are: fuel cell power system, DC–DC converter, battery, electric motor and transmission system. The fuel cell power system which is comprised of fuel cell stack and auxiliary components are modeled and simulated in a previous paper by the authors. The fuel cell is controlled so that it operates at its peak net power. Depending on driving condition, the stack temperature changes during the vehicle performance. To prevent the temperature from exceeding a limit, which is 80 °C, a PID controller is employed. The results of the power system modeling are validated using a previous study on a polymer electrolyte membrane fuel cell power system in K.N. Toosi University of Technology. The hybrid configuration of the vehicle improves its performance in acceleration, slope climbing, extending the driving range and fuel consumption. The battery state of charge (SOC) should always remain in a prescribed range. In this study, the battery SOC is controlled within its defined range during vehicle performance using two controllers. Finally, fuel consumption and vehicle performance are investigated during two driving cycles.

List of symbols

A	Vehicle frontal area/m^2
a	Acceleration/m s^{-2}
c	Drag coefficient, air specific heat/J mol^{-1} K^{-1}, capacitance/J K^{-1}
E	Open circuit voltage/V, equilibrium potential/V
F	Force/kN, Faraday number/Coulombs
f	Friction coefficient
g	Gravity acceleration/m s^{-2}
H	Heat flow rate/J s^{-1}
h	Hydrogen enthalpy/J kg^{-1}, heat transfer coefficient/W m^{-2} K^{-1}
I	Current/Amp
J	Inertia/kg m^2
k	Conversion factor
LHV	Lower heating value/kJ kg^{-1}
m	Mass/kg
n	Number of stack cells, number of battery cells
p	Pressure/Pa
P	Power/kW
Q	Flow rate/kg s^{-1}
q	Capacity/Ah
r	Radius/m
R	Gas constant/J kg^{-1} K^{-1}, battery internal resistance/Ω
SOC	State of charge
T	Temperature/K
u	Control input/V
V	Volume/m^3
v	Voltage/V
vel	Velocity/km h^{-1}

A. Yazdani · A. H. Shamekhi · S. M. Hosseini (✉)
Mechanical Engineering Faculty, K.N. Toosi University of Technology, Tehran, Iran
e-mail: mehdi.hosseini64@gmail.com

Greek letters

Γ	Gear ratio
α	Path slope/rad, current compensation coefficient for the discharge curve
β	Temperature compensation coefficient for the battery curve
γ	Air specific heat ratio
Δ	Variation
η	Efficiency
λ	Temperature compensation coefficient
μ	Power converter coefficient
ρ	Density/kg m^{-3}
τ	Torque/kN m, Time delay constant/s
ω	Rotational speed/rad s^{-1}

Subscripts

0	Initial
a	Air
accel	Acceleration
act	Activation
an	Anode
atm	Atmospheric
batt	Battery
bus, DC	DC BUS
c	Converter
ca	Cathode
cu	Current
cm	Compressor motor
conc	Concentration
cool	Cooling system
cool_water	Cooling water
cp	Compressor
d	Drag
dc	DC–DC converter
elec	Electrical load
fc	Fuel cell
fm	Feed manifold
g	Generator
gr	Gradient
in	Inlet
loss	Loss through stack surface, losses
m	Electric motor
net	Net
ohm	Ohmic
p	Pressure
roll	Rolling
st	Stack
t	Thermal
tot	Total
tr	Traction
v	Vapor
veh	Vehicle
w	Wheel

1 Introduction

Internal combustion engines are one of the major sources of fuel consumption and pollutant emission. In recent years, hybrid vehicle technology has developed due to rising fuel prices and environmental problems. Although hybrid vehicles have less fuel consumption and greenhouse gas production, they still have the problem of fossil fuel consumption. Therefore, the importance of study on new energy sources and investment on electric and fuel cell vehicles is obvious [1]. FCs are currently one of the focus points of automotive industries as an alternative to conventional internal combustion engines. Among all FC types, the polymer electrolyte membrane fuel cell (PEM-FC) has proved to be a prime candidate and the most appropriate technology in vehicle applications due to satisfactory efficiency and low operating temperature (25–90 °C). This low operating temperature reduces the start-up time and transience [2–4]. Moreover, they have high power density, low corrosion, less sediment, relatively long cell and stack life and solid electrolyte [5–8]. Application of energy storage systems (ESS) to optimize Power usage is usual in fuel cell vehicles [9]. These sources are capable of storing the energy produced by regenerative braking and providing a division of power required as a supporting system for fuel cell when needed. Since transient loads decrease the fuel cell stack life considerably, taking advantage of these sources is a helpful solution to prolong the cell durability. The division of the load between the fuel cell and the storage source is the task of a controller. When the state of charge (SOC) of the storage source is low, the fuel cell is responsible for both providing the required load and charging the storage source. On the other hand, when the SOC of the storage source is high enough and the vehicle is accelerating or slope climbing, this source must support fuel cell. Two common energy storage devices are batteries and ultracapacitors. In this study, a Li-ion battery is used as the energy storage source. These types of batteries are considered as one of the best rechargeable batteries and their use in electric vehicles is very successful [10].

The configuration of the hybrid vehicle in this study is depicted in Figs. 1 and 2. The fuel cell power system used here is totally modeled and simulated. Major elements are air compressor, fuel cell stack (comprised of cathode, anode and membrane) and stack cooling system [11]. In this system, hydrogen (which is stored in a high-pressure tank) is injected to anode. On the other side, the compressed air (which is cooled and humidified due to its high temperature) is injected to cathode. In the stack, chemical reactions take place and electrical current as main product and heat and water as byproducts are produced [12–15].

**Fig. 1** A schematic view of the hybrid fuel cell electric vehicle components
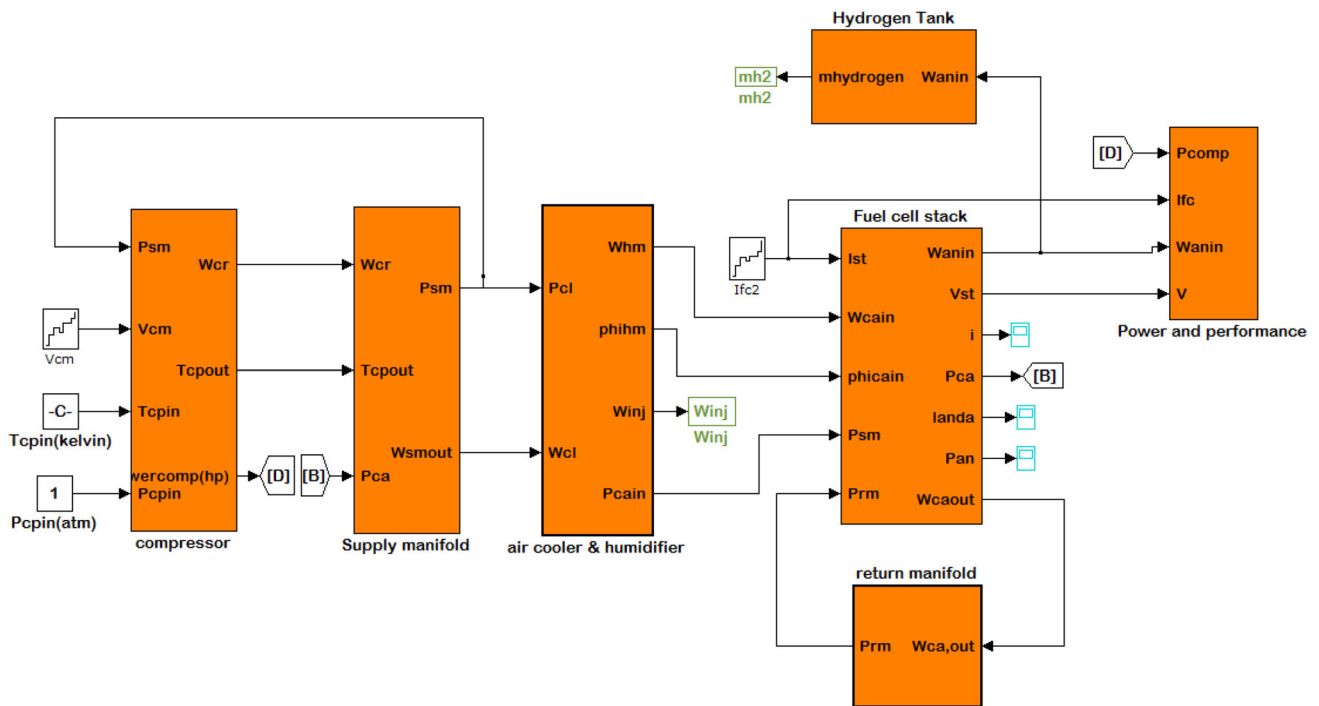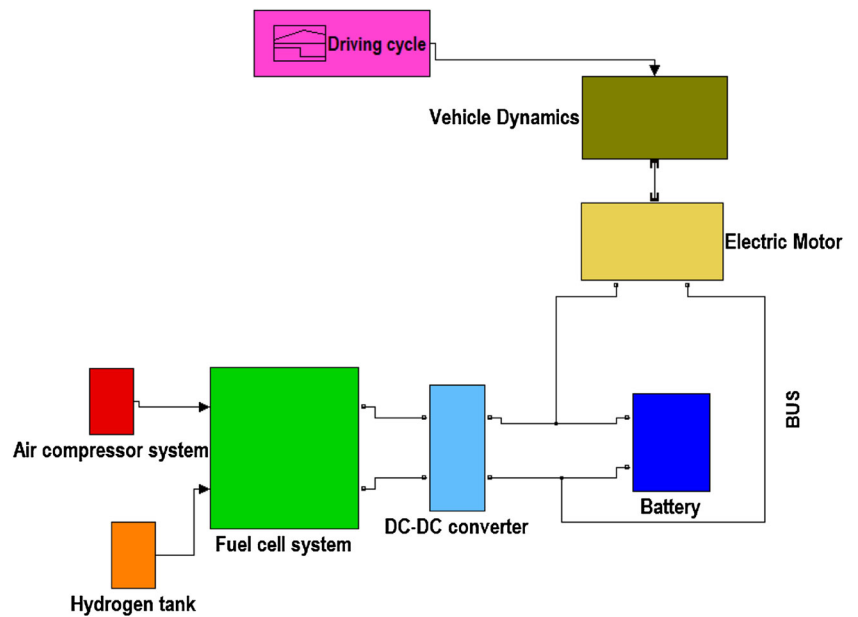
Fig. 2 A schematic view of fuel cell power system model

The variation of stack temperature is an important issue which must be controlled properly. The desired limit of temperature of the PEMFC in this model is considered to be 80 °C. The cooling system is made up of a heat exchanger with coolant. The input of this system is cooling system voltage. While the current drawn from cell increases, the temperature increases; so two inputs play the role in altering system temperature: (1) fuel cell current and (2) cooling system voltage.

The variations of electric current drawn from fuel cell affect its terminal voltage. This characteristic is illustrated as fuel cell polarization curve. It demonstrates fuel cell voltage versus cell current density (which is defined as current per unit cell active area). In Fig. 3, a polarization curve of a specific PEM fuel cell is depicted. The large variation of cell terminal voltage and consequently BUS voltage is not desired and leads to perturbation in the performance of the electric motor; hence, the use of a DC–

Fig. 3 Polarization curve of a specific PEM fuel cell at 70 °C [16]
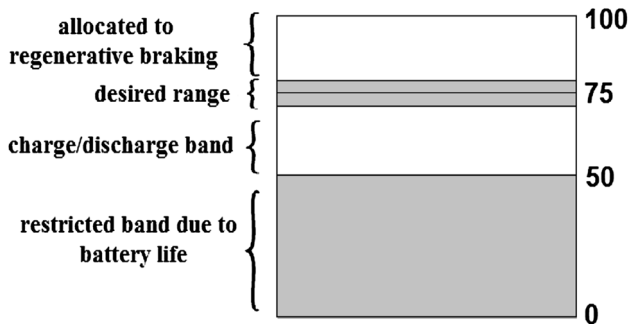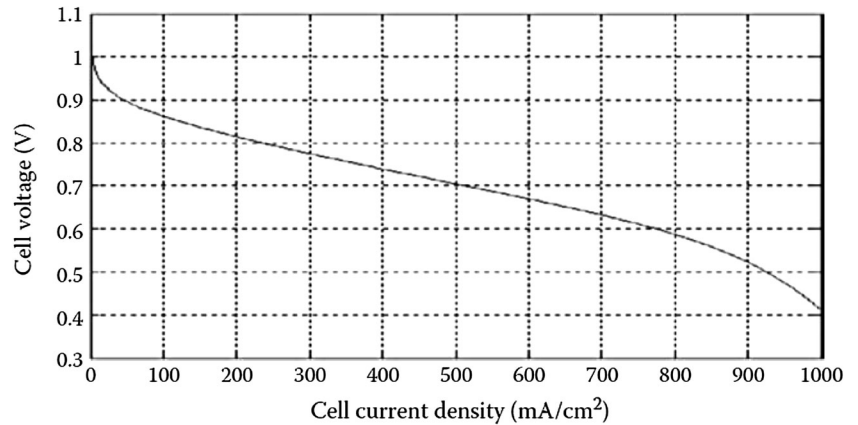
Fig. 4 Different bands of battery state of charge (SOC)

DC converter (which is an electrical circuit converting the voltage of a direct current source to another level of voltage) seems inevitable.

As mentioned, battery is used both as an auxiliary and storage source. Battery assists fuel cell when it is unable to produce required traction power of the electric motor and stores energy of the regenerative braking. Battery life imposes restrictions for its available energy and its SOC must remain in a confined range. When SOC is almost zero, the number of cycles of charge/discharge is dramatically reduced [17]. Batteries have three important SOC levels which are:

- Maximum SOC which is generally considered as 100 %
- Desired SOC
- Minimum SOC

As shown in Fig. 4, the minimum SOC is 50 % and the desired level of SOC is 75 %. The SOC desired band includes three percents higher and lower than the desired level and depends on the driving cycle and the ability of the control system of battery charge. At SOCs higher than the desired level, the battery is never charged by the command of the control system and this band is allocated to regenerative braking. At SOCs between the desired range and the restricted band, the battery can either be charged up to the

desired level or discharge to SOC of 50 %. In this range, the battery assists fuel cell and supplies a division of the traction motor demanded power.

The paper is organized as follows: in Sect. 2, modeling of the elements of the hybrid vehicle is presented; Sect. 3 deals with simulating, validating and controlling of the FC power system; in Sect. 4, the hybrid fuel cell vehicle is simulated and battery SOC is controlled. Also, in this section, vehicle performance during two driving cycles is studied and the results, in terms of fuel consumption, are presented in a table. Finally, in Sect. 5, the conclusions are discussed.

2 Modeling of the hybrid fuel cell electric vehicle

In this section, all components of the vehicle power train system are modeled. The fuel cell power system is completely modeled and simulated in [11]. Here, the most important relationships are brought.

2.1 Fuel cell power system submodel

The air supply subsystem inputs are temperature and pressure of ambient air, compressor voltage and cathode pressure. Compressor speed and pressure at each stage are the only state variables. The air compressor dynamics can be described by the following equation:

$$P_{cp} = \frac{c_p T_{atm}}{\eta_{cp} \eta_m} \left[\left(\frac{p_{fm}}{p_{atm}} \right)^{\frac{\gamma-1}{\gamma}} - 1 \right] Q_{cp} \tag{1}$$

The stack voltage can be obtained by the following equations:

$$v_{st} = n_{st} v_{fc} \tag{2}$$

$$v_{fc} = E - v_{act} - v_{ohm} - v_{conc} \tag{3}$$

Obtained voltage from Eq. (4) is theoretical and it is about 1.2 V for a cell operating below 100 °C. The open circuit voltage is a little less than theoretical voltage. In this

study, we consider three main losses which cause significant voltage drop.

(i) The ohmic membrane loss arises from polymer membrane resistance to the proton transfer and the ohmic resistance of the external circuit.

(ii) Concentration loss, caused by back diffusion of reactants of cathode. The reason of sudden voltage drop at high current density is concentration loss.

(iii) Activation loss arises from the energy needed to break and form new bonds in the anode and cathode side [11]. This part of energy is used to drive the chemical reactions.

$$E = 1.032 + 4.3085 \times 10^{-5} T_{st} \times [\ln(p_{H_2})$$
$$+ \frac{1}{2} \ln(p_{O_2}) - \ln(p_{v,ca})] \tag{4}$$

The heat management is one of the significant factors in fuel cell stack which guarantees the temperature to be at the desired value. It is directly related to the fuel cell performance. The stack cooling system can be modeled by the following equations:

Transient energy balance is expressed by the Eq. (5).

$$H_{st} = c_t \frac{dT_{st}}{dt} = P_{tot} - P_{elec} - H_{cool} - H_{loss} \tag{5}$$

The heat removal rate by the cooling water can be calculated by Eq. (6).

$$H_{cool} = Q_{cool\_water} \cdot c_p \cdot \Delta T_{st} \tag{6}$$

The rate of heat loss by the stack surface can be obtained from Eq. (7).

$$H_{loss} = h A_{st} \cdot (T_{st} - T_{atm}) \tag{7}$$

2.2 DC–DC converter submodel

Due to driving cycle or battery needed to be charged, current drawn from fuel cell may change frequently. As stated before, these variations affect the terminal voltage of the cell, BUS voltage and traction motor performance which is not favorable; as a result, since the current generated by fuel cell is DC, a DC–DC converter is employed.

Because of converter fast dynamics, it is assumed to be static and described by the following model [18]:

$$P_{dc} = \eta_{dc} \cdot P_{fc} \tag{8}$$

So, the following equation holds in vehicle power system:

$$P_{desired} = P_{dc} + P_{batt} \tag{9}$$

2.3 Battery submodel

One type of common batteries in electric vehicles is Li-ion battery. In this study, a Li-ion battery model available in Matlab/Simulink is employed. The battery parameters are presented in simulation section.

A model of Li-ion battery is given here [19]:

$$I_{batt}(t) = \frac{P_{batt}(t)}{v_{batt}(t) \cdot n_{batt}} \tag{10}$$

$$E(t) = v_{batt}(t) - R_{batt} \cdot I_{batt}(t) \tag{11}$$

$$v_{batt} = n_{batt} \cdot \sum_{k=0}^{n} C_k \cdot \left(1 - SOC^k(t)\right) + \lambda(T_{batt}(t)) \tag{12}$$

$$SOC(t) = 1 - SOC_0$$
$$+ \frac{1}{q_{batt}} \int_{0}^{t} \alpha_{cu}(I_{batt}(t)) \cdot \beta(T_{batt}(t)) \cdot I_{batt}(t) dt \tag{13}$$

2.4 Vehicle system submodel

In this section, vehicle dynamics and its force balance are modeled to calculate the demanded traction power during driving cycle. The output of this model is demanded traction power and the input is driving cycle (speed profile); driving cycle is defined as vehicle speed, acceleration and the slope of the road. Speed profile data are acquired from Advisor© software library which includes many driving cycles with velocity values as arrays. These arrays then can be introduced in Simulink as an input. Acceleration profile is calculated from speed profile by the following equation:

$$a = \frac{dvel}{dt} \tag{14}$$

The vehicle force balance equation is [20]:

$$F_{tr} = m_{veh} \cdot a + F_{air} + F_{roll} + F_{gr} \tag{15}$$

where, F_{tr} is the vehicle traction force (N), m_{veh} is the vehicle mass, F_{air} is air resistance, F_{roll} is the friction force and F_{gr} is the gravity force.

Traction torque and rotational speed of the wheel are determined by:

$$\tau_w = F_{tr} \cdot r_w \tag{16}$$

$$\omega_w = \frac{vel}{r_w} \tag{17}$$

2.5 Electric traction motor and transmission submodel

In this study, the electric traction motor is a permanent magnet synchronous motor (PMSM). A single-ratio gearbox and a differential gear with the ratio of 1.0, transfer the motor torque to the rear wheels. This motor acts as a generator during regenerative braking. Transmission system equations are:

$$\omega_m = \omega_w \cdot \Gamma \tag{18}$$

Fig. 5 Fuel cell current
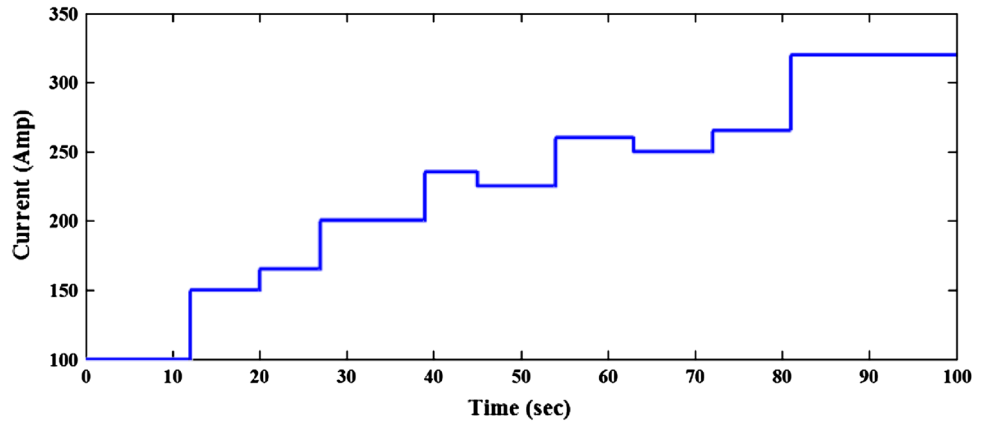
$$\tau_{\mathrm{m}} = \frac{\tau_{\mathrm{w}}}{\Gamma} \tag{19}$$

The electric traction motor is modeled by following equations:

$$P_{\mathrm{m,net}} = \tau_{\mathrm{m}} \cdot \omega_{\mathrm{m}} \tag{20}$$

$$P_{\mathrm{m,loss}} = \begin{cases} 0.016 \cdot \tau_{\mathrm{m}}^2 + 8.2 \cdot 10^{-3} \cdot \omega_{\mathrm{m}}^{1.5} & \text{if } \omega_{\mathrm{m}} > 210 \\ 4.05 \cdot 10^{-9} \cdot \tau_{\mathrm{m}}^2 \cdot \omega_{\mathrm{m}}^2 + 8.2 \cdot 10^{-3} \cdot \omega_{\mathrm{m}}^{1.5} & \text{if } \omega_{\mathrm{m}} \leq 210 \end{cases} \tag{21}$$

$$P_{\mathrm{m}} = \begin{cases} P_{\mathrm{m,net}} \cdot \eta_{\mathrm{g}} & \text{if } P_{\mathrm{m,net}} \leq 0 \\ P_{\mathrm{m,net}} + P_{\mathrm{m,loss}} & \text{if } P_{\mathrm{m,net}} > 0 \end{cases} \tag{22}$$

The fuel cell and the battery generate direct current and since the electric motor is a PMSM, a DC–AC converter is employed to convert direct current of the BUS to alternative current which is fed to the motor. Due to having fast dynamics, this converter is assumed to be static and modeled by the following equation:

$$P_{\mathrm{bus,DC}} = \frac{P_{\mathrm{m}}}{\mu_{\mathrm{c}}} \tag{23}$$

3 Simulation results and control of the fuel cell power system

In this section, the FC power system simulation results are given. Also, fuel cell temperature and net system power are controlled. At the end, simulation results are validated. All the simulation results are generated by Matlab/Simulink software.

3.1 Fuel cell power system simulation

By applying three inputs to the model, variations of many parameters in the fuel cell system can be monitored. These inputs are: fuel cell current, compressor voltage and cooling system voltage (the values of these inputs are different from those presented in [11]). These inputs are shown in Figs. 5, 6 and 7, respectively.

By applying these inputs to the model, Figs. 8, 9, 10, 11, which are the most significant outputs, are obtained. In Fig. 7, fuel cell stack temperature variations, during simulation, are illustrated. Two main factors affecting the temperature, are cooling system voltage and current drawn from stack. In this figure, until almost 35th s, the cooling system is off but since the current is increasing, the temperature rises too. On the other hand, at 90th s, the current is constant but due to a large increase in cooling system voltage, the temperature tends to reduce.

Figure 9 shows fuel cell power, system net power and compressor consumed power. System net power is defined as the difference between fuel cell power (gross power) and compressor consumed power (Eq. 24).

$$P_{\mathrm{net}} = P_{\mathrm{gross}} - P_{\mathrm{cp}} \tag{24}$$

At the end of the simulation, where the compressor consumed power is maximum, almost a difference of 13 kWs exists between fuel cell power and system net power.

Variations in fuel cell efficiency are demonstrated in Fig. 10; efficiency is defined as follows:

$$\eta = \frac{P}{Q_{H_2,\mathrm{an,in}} \mathrm{LHV}_{H_2}} \tag{25}$$

Although FC power increases, after 50th s, unexpectedly, system efficiency does not improve much. This is because of high ohmic, concentration and activation losses in the fuel cell stack. At high currents, compressor consumed power increases dramatically. For this reason, it is preferred that the system operates at low currents and high voltages to minimize system losses and efficiency drop. But in a vehicle in motion, that the current drawn from power system is subject to frequent changes, practically, it is impossible for the system to operate at low currents. As a result, awareness of the performance of fuel cell and utilizing the information available in polarization curve can be beneficial in designing a vehicle power system.
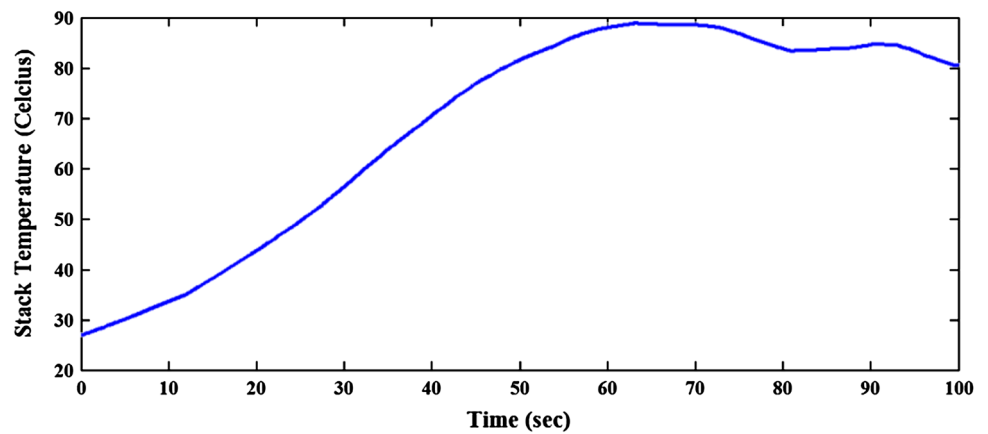
Fig. 6 Compressor voltage
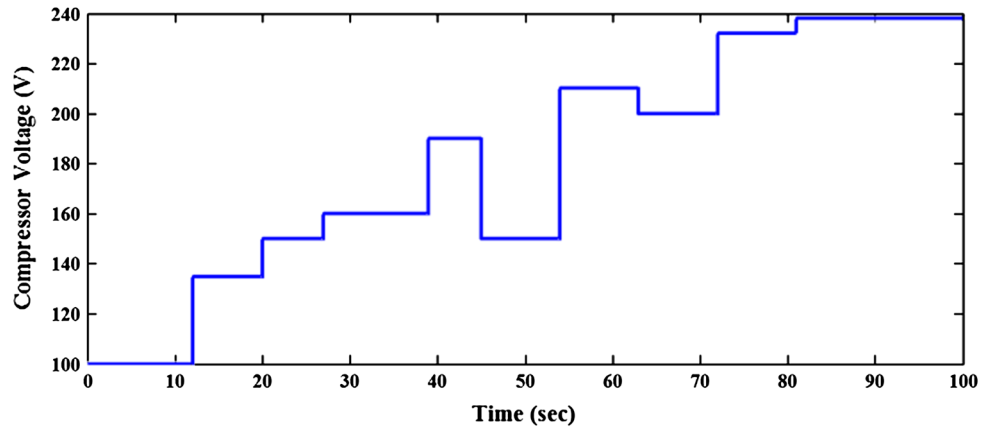
Fig. 7 Cooling system voltage
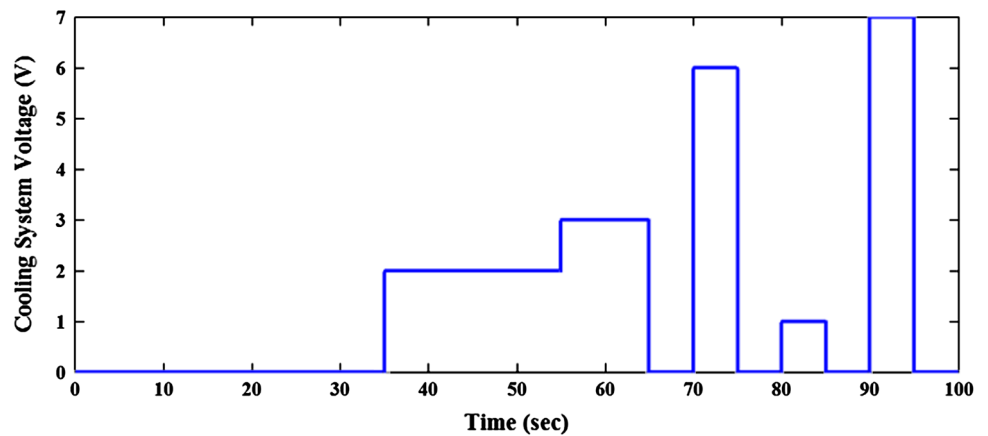
**Fig. 8** Fuel cell stack temperature variations

In Fig. 11, the fuel cell net power versus compressor voltage, at different currents, is shown. This figure also indicates that, at a constant current, by increasing compressor voltage, system net power first improves due to oxygen partial pressure increase in cathode; however, it drops from a specific voltage because of compressor excessive consumed power. This deficiency is dealt with in fuel cell power control section.

3.2 Fuel cell power control

As mentioned before, at a constant current, by increasing compressor voltage, system net power improves first but then drops; so the net power curve has a maximum value at each current. The target of control system here is selecting the compressor voltage so that the net power is maximized. In addition, based on Eq. (25), at a constant current and

382

J Braz. Soc. Mech. Sci. Eng. (2015) 37:375–396

Fig. 9 Fuel cell, compressor and system net powers variations
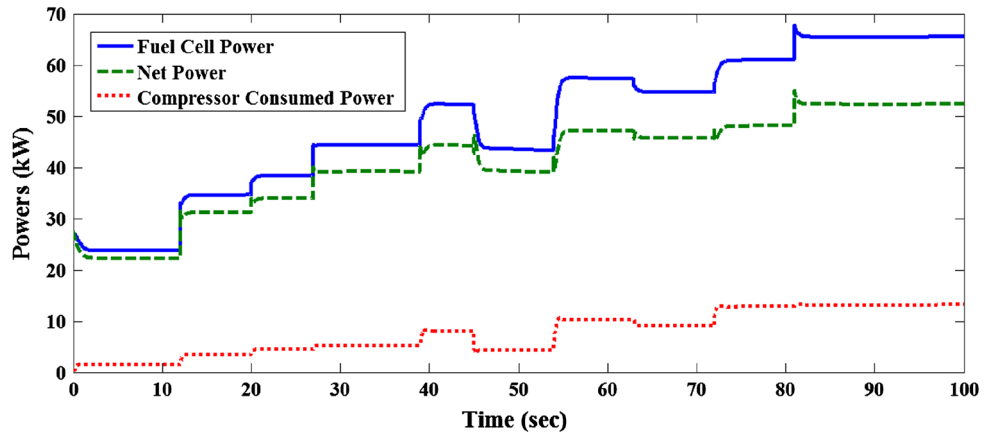
Fig. 10 Fuel cell and system efficiencies variations
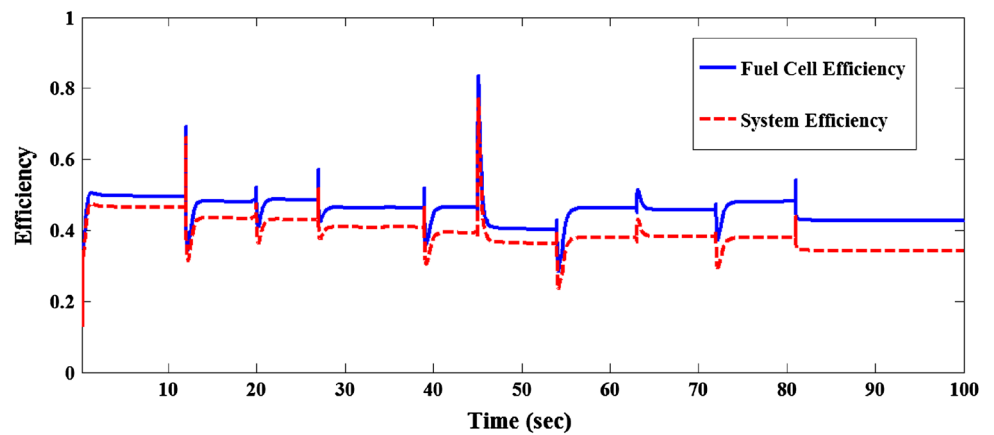
Fig. 11 Variations of system net power versus compressor voltage at different currents
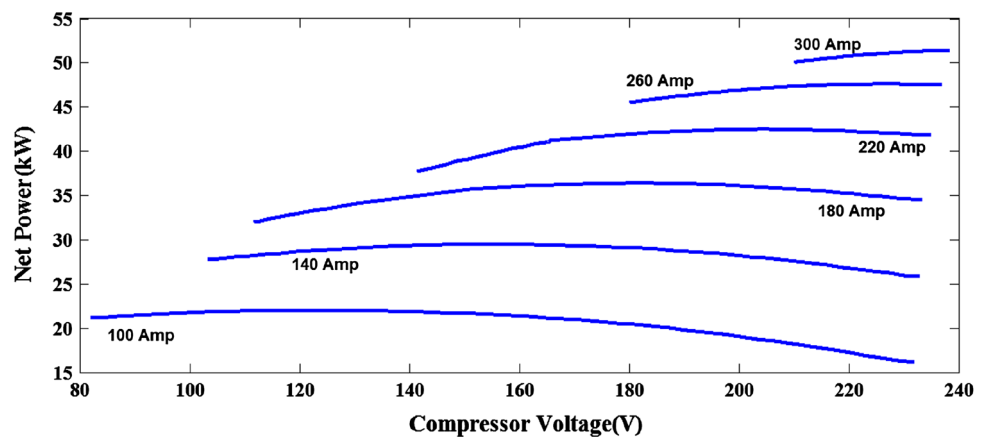
compressor voltage, when the net power is maximized, the system net efficiency has its maximum value.

Here, considering Fig. 11, for each current from 100 to 300 amp, the compressor voltages which make the system net power maximum, are selected and arranged a look-up table which is in fact a static controller. Figure 12 displays this controller.
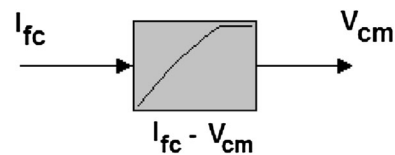
Fig. 12 Look-up table schematic

Fig. 13 Comparison between fuel cell system net power with and without controller
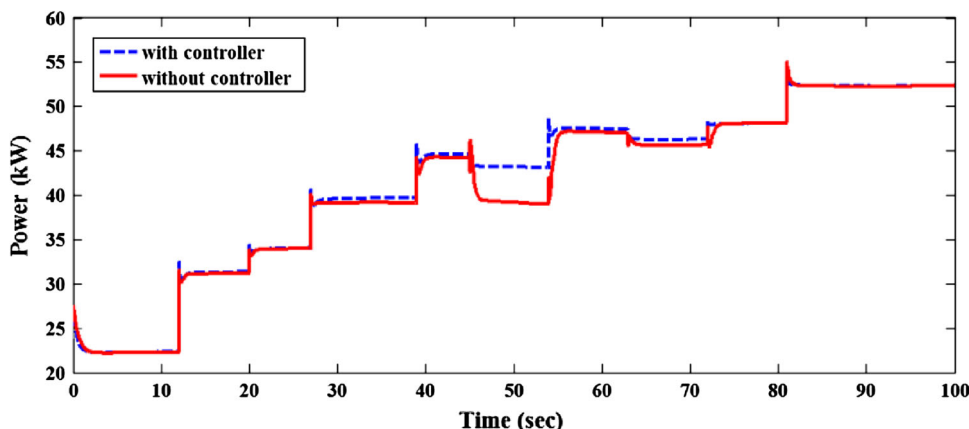
Now, by employing this look-up table in the model and applying two inputs of current and cooling system voltage (Figs. 5 and 7, respectively), system net power variation can be monitored. The system performance using this controller and using compressor voltage input (depicted in Fig. 6), are simulated separately and are illustrated in Fig. 13.

Figure 13 shows that in the time period between 27 and 70th s, using the controller leads to more system net power. At instants that the two powers, with controller and without controller, turn out to be exactly equal, the compressor voltage in Fig. 6 is accidentally equal to the voltage obtained from look-up table.

As a result, obtained compressor voltage from look-up table is optimized as a function of maximum FC system net power. So, hereafter this look-up table is always utilized to assign compressor voltage for each fuel cell current.

3.3 Fuel cell temperature control

Temperatures higher than 80 °C may damage fuel cell stack membrane, so the purpose of temperature control is to prevent from these damages. Two parameters play a major role in changing cell temperature: fuel cell current and cooling system voltage. Stack temperature dynamic has a greater time constant than other dynamics in the system; therefore, using a local controller can be useful. Here, a PID controller is employed, the coefficients of which are calculated with trial and error method so that the temperature does not exceed 80 °C. The controller input is the deviation of the stack temperature from the reference value (80 °C). Its output is cooling system voltage. This voltage is limited between 0 and 10 V which is the allowed range for cooling pump.

The stack temperature may have a value lower than 80 °C, depending on fuel cell current and heat loss through
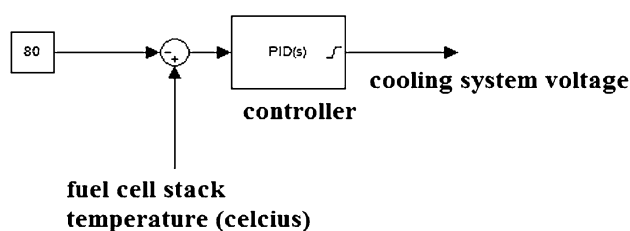
Fig. 14 A schematic view of fuel cell stack temperature controller

stack surface (in the beginning of simulation, stack temperature is equal to ambient temperature). Cooling system starts working just when the temperature exceeds the limit. Figure 14 shows a schematic view of stack temperature controller.

By applying the inputs of current and compressor voltage (Figs. 5 and 6, respectively), stack temperature variations are compared separately; once with the PID controller and once without it (with the cooling system voltage input in Fig. 7). The results are illustrated in Fig. 15. In this figure, it is noticed that from almost 45th s the controller has maintained the temperature on 80 °C level. Without this controller, the temperature increases to 88 °C which is not favorable.

The controller output which is the cooling system voltage is depicted in Fig. 16.

In this figure, it is noticed that until 42th s, that the temperature is lower than 80 °C, the voltage applied to the cooling pump by the controller is zero and then it reaches its top allowable value of 10 V.

Now, by utilizing these two controllers (power and temperature), the polarization curve of this fuel cell is obtained and shown in Fig. 17. As mentioned before, this curve plots stack voltage versus cell current density; current density is current per unit cell active area. It is seen in Fig. 17 that increase in current and in turn, cell current density, causes decrease in stack voltage.
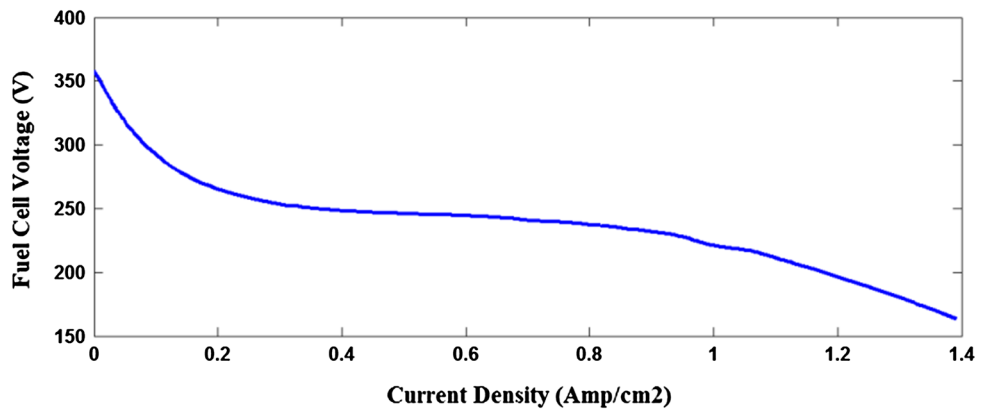
384

J Braz. Soc. Mech. Sci. Eng. (2015) 37:375–396

Fig. 15 Comparison between fuel cell stack temperature with and without controller
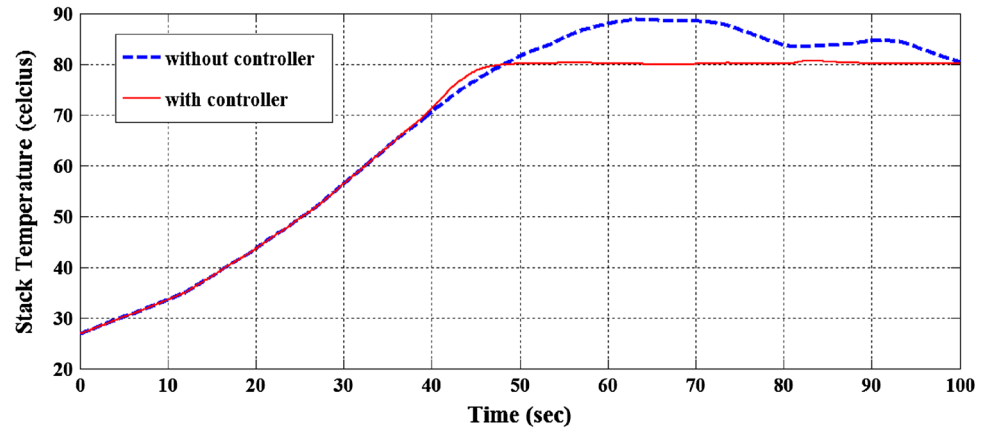
Fig. 16 Cooling system voltage during the simulation (controller output)
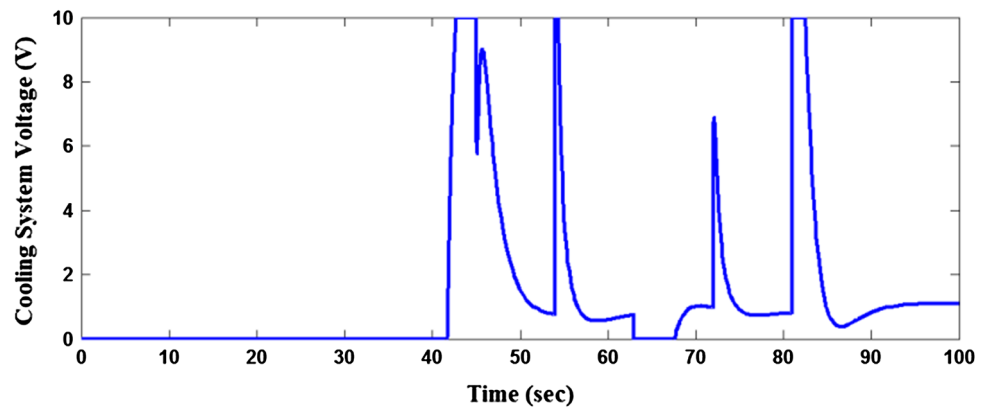
**Fig. 17** Fuel cell polarization curve

This decrease in stack voltage is because of concentration loss and leads to fuel cell power and efficiency drop as it can be seen in Fig. 18.

As shown in Fig. 18, in current densities higher than 0.9, a drop in FC efficiency happens. Therefore, to maintain appropriate efficiency and reduce fuel consumption, the current must be confined to this allowable limit which, for the fuel cell under study, is equal to 252 amp. In the hybrid vehicle, at high traction motor currents, auxiliary source such as battery compensates for this restriction in fuel cell operation.

3.4 Simulation results validation

Because no data of the fuel cell system modeled are available for validation, this model is adapted for a Nexa PEM 1.2 kW fuel cell power module as much as possible. This module is accessible in the power laboratory in electrical engineering faculty of K.N. Toosi University of Technology. This fuel cell is composed of 47 cells and its experimental results are proposed in [21]. The model is calibrated with the temperature profile and the calibration is done with stack drawn current of 25.5 (A). The
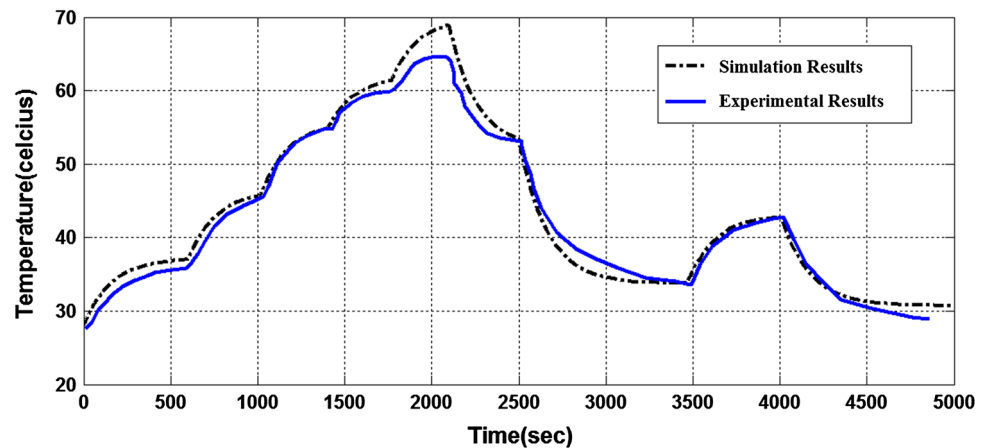
Fig. 18 Fuel cell efficiency versus current density
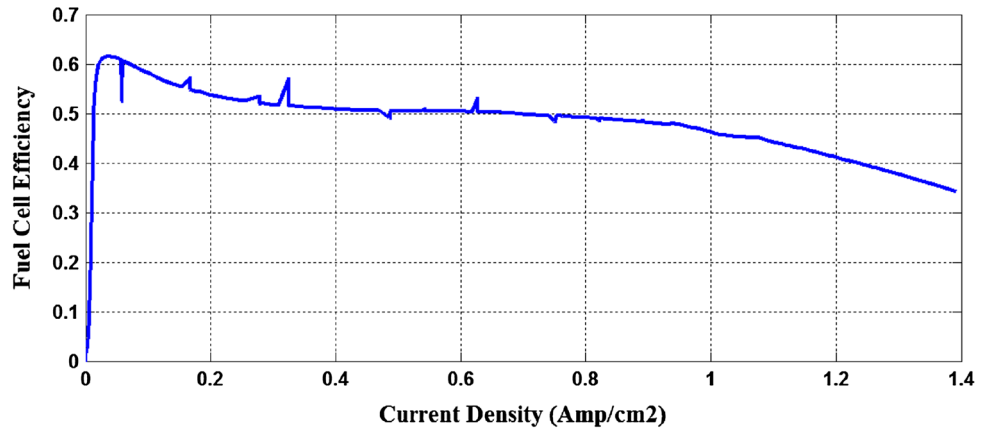
Fig. 19 Comparison between stack simulated and experimental temperatures at different currents
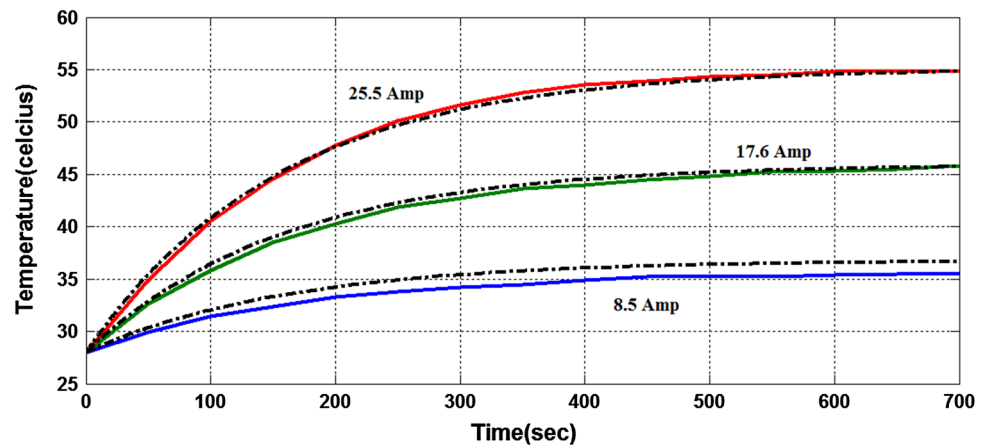
Fig. 20 Comparison between experimental and simulation results of stack temperature

comparison between experimental and simulation results is demonstrated in Fig. 19.

As noticed in Fig. 19, temperature response at stack currents of 17.6 and 8.5 amp has good compatibility with experimental results.

By applying the step in current proposed in [21], the simulated results for temperature response and stack terminal voltage are depicted in Figs. 20 and 21.

Figure 20 shows good harmony between simulation and experimental results. The maximum difference in results takes place in almost 2,000th s which leads to 6 % error.

The simulated and experimental terminal voltage of fuel cell stack is illustrated in Fig. 21. At lower stack voltages (high stack drawn current), there is good agreement in results. But, at some instants, the value of the error increases to 9.8 % which can be justified by this fact that

Fig. 21 Comparison between experimental and simulation results of stack terminal voltage
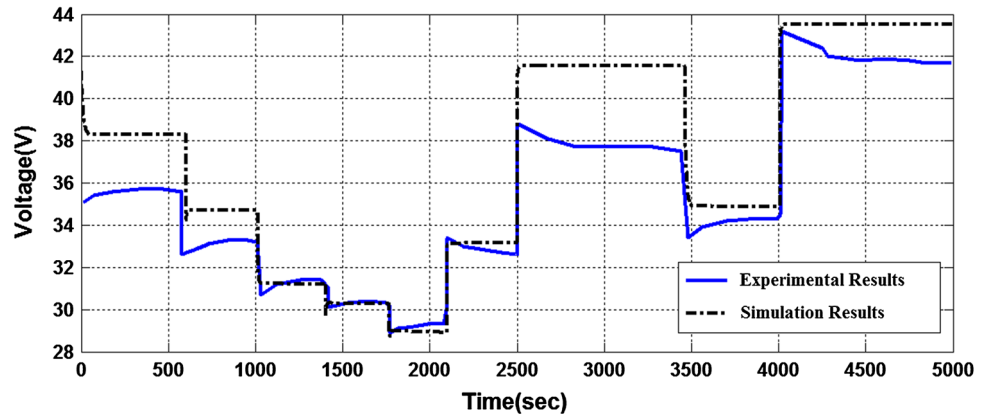
Table 1 Parameters used in hybrid fuel cell vehicle simulation

Parameter	Value	Parameter	Value	Parameter	Value
ρ_{air}	1.199 kg m^{-3}	f_{roll}	0.0124	Tire	185/65 R15
c_d	0.26	m_{veh}	1,500 kg	V_{batt}	288 V
A_{veh}	2.7 m^2	Γ	7.2	Q_{batt}	12.57 Ah
Vehicle track	1,720 mm	Vehicle length	4,527 mm	Fuel cell	320 cells 80 W
Wheelbase	2,671 mm	Vehicle height	1,460 mm	Electric motor	80 kw 288 V

Fig. 22 Vehicle speed input
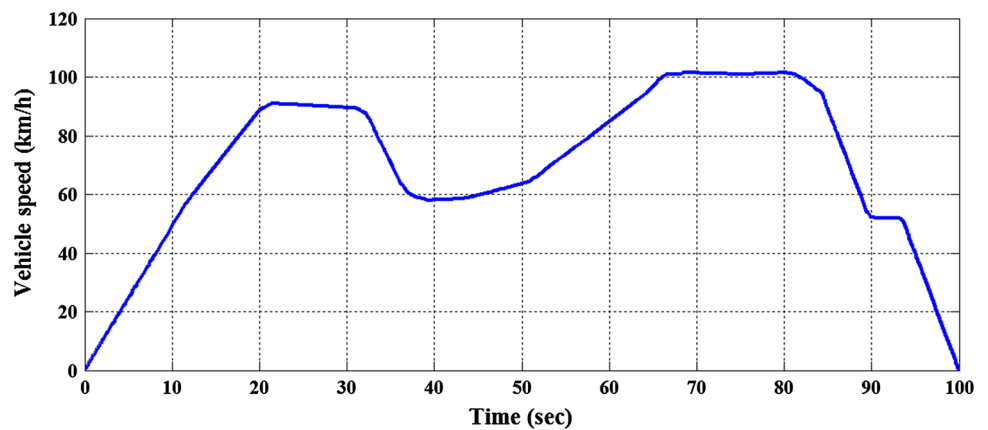
the auxiliary components such as air compressor are different in the model and the experiment setup. Better results would be obtained if clear information was available about the components of the Nexa power system.

4 Simulation results and control of the hybrid fuel cell vehicle

4.1 Hybrid fuel cell vehicle simulation

This section presents the simulation results of the hybrid fuel cell vehicle model using Matlab/Simulink software. Vehicle simulation parameters used in this model are listed in Table 1.

In this simulation, the initial values of hydrogen mass in the tank and battery SOC are assumed 1.5 kg and 60 %, respectively. Since the battery SOC is not controlled yet, the battery is only charged by regenerative braking.

The inputs to this model are road slope and vehicle speed and acceleration. The acceleration is calculated from vehicle speed, so two inputs of road slope and vehicle speed are applied to the model and the hybrid vehicle performance is investigated. The road slope is assumed to be constant and equal to 15 % during this simulation. Figure 22 shows the vehicle speed input.
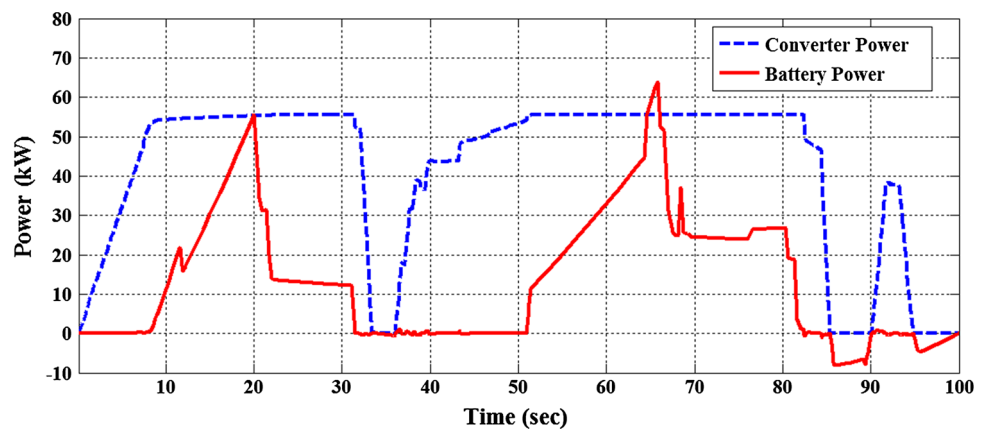
Figure 23 shows traction motor power and Fig. 24 illustrates DC–DC converter and battery powers.

In fig. 24, the electric power of two sources for providing vehicle traction power (which are DC-DC converter,
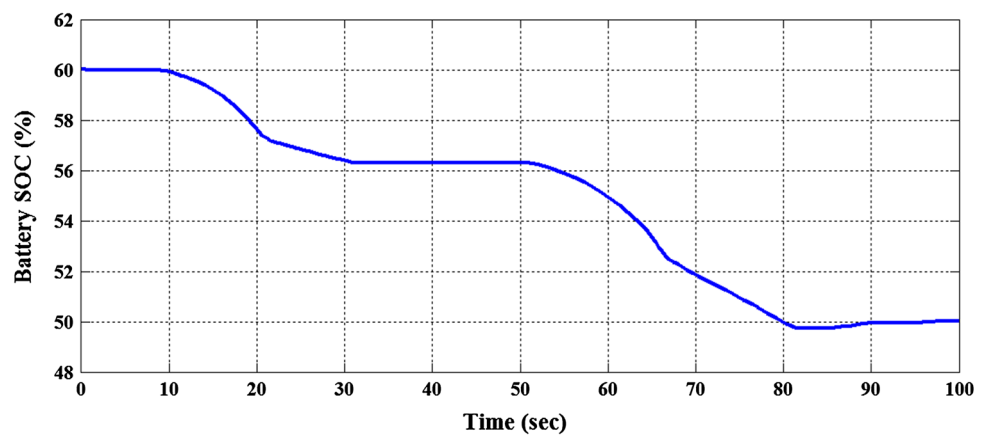
Fig. 23 Electric motor demanded power
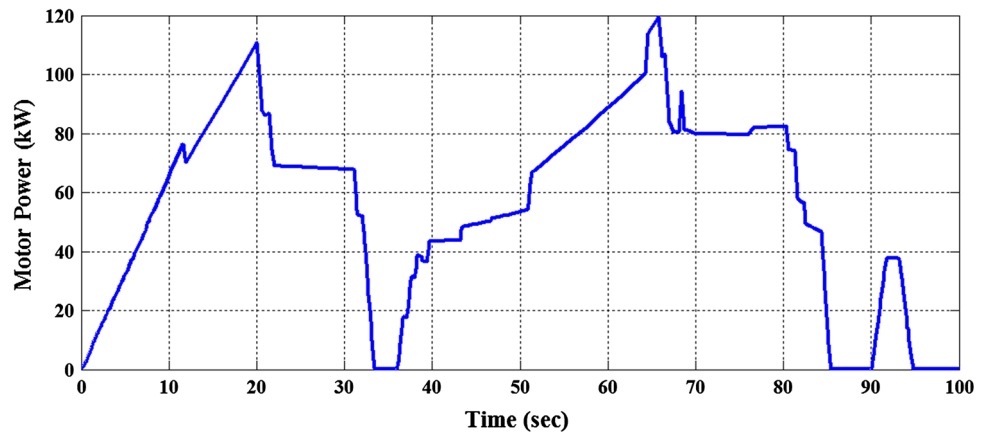
Fig. 24 DC–DC converter and battery power

**Fig. 25** Battery SOC variations

with the input current delivered by fuel cell, and battery) are displayed. The converter power is always non-negative, whereas battery power is positive during discharge and negative while the battery is being charged. In this figure, the battery is charged by regenerative braking; at the final instants of the simulation, regenerative braking makes the SOC rise, as it can be seen in Fig. 25. Except the instants that battery power is negative, it is apparent that, at any

time, the sum of battery and converter powers is equal to the electric motor required traction power.

In Fig. 25, at $t = 80$ s, the SOC drops lower than 50 % and is increased slightly due to regenerative braking and remains by the level of 50 %. In this condition, in case more current is drawn from battery, the SOC will be in the restricted band, which was mentioned previously, and will not recover significantly. In the following section, by

388

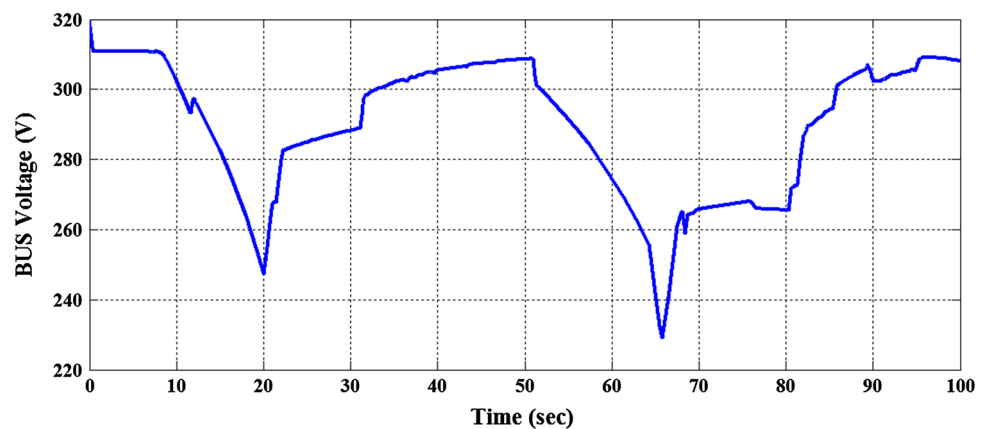J Braz. Soc. Mech. Sci. Eng. (2015) 37:375–396

Fig. 26 Current drawn from fuel cell
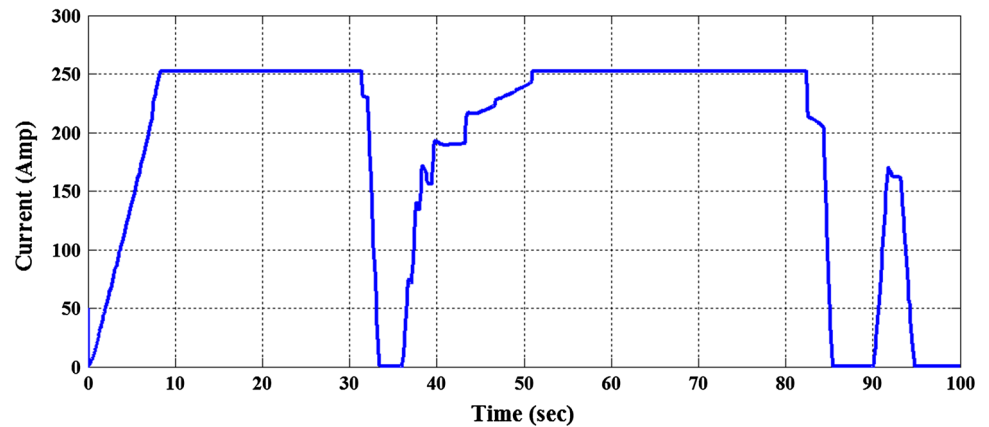
Fig. 27 Fuel cell terminal voltage
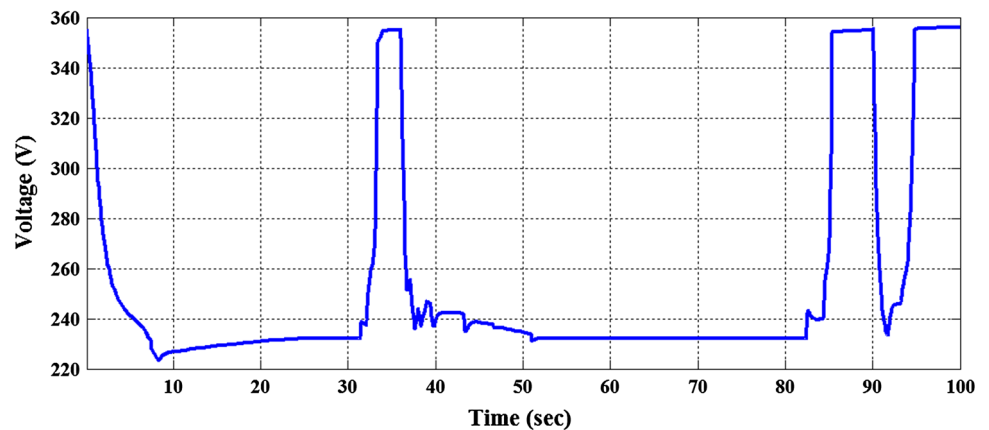
Fig. 28 DC current BUS voltage

employing a controller, battery SOC will be governed in a favorable range.

In Fig. 26, current drawn from fuel cell is depicted. As it was mentioned in previous section, fuel cell current must not exceed an allowable range; otherwise the losses will rise dramatically. In this figure, it can be seen that the limit of 252 amp, specific for this fuel cell, is the maximum allowable current.

Fuel cell terminal voltage is displayed in Fig. 26. It is apparently seen that, at some instants, the voltage variation is very large which is not desirable; for this reason the DC–

DC converter is used in the circuit (Fig. 27). In Fig. 28, the voltage of this converter, which is equal to the DC current BUS voltage, is illustrated. It is obvious that at the instants where the fuel cell terminal voltage has large variations (for example between $t = 30$ and 40 s), the BUS voltage changes slightly.

Hydrogen fuel consumption during the simulation is shown in Fig. 29. At the instants that the current drawn from fuel cell stack has the lowest possible values, due to vehicle speed and road slope, hydrogen mass does not change
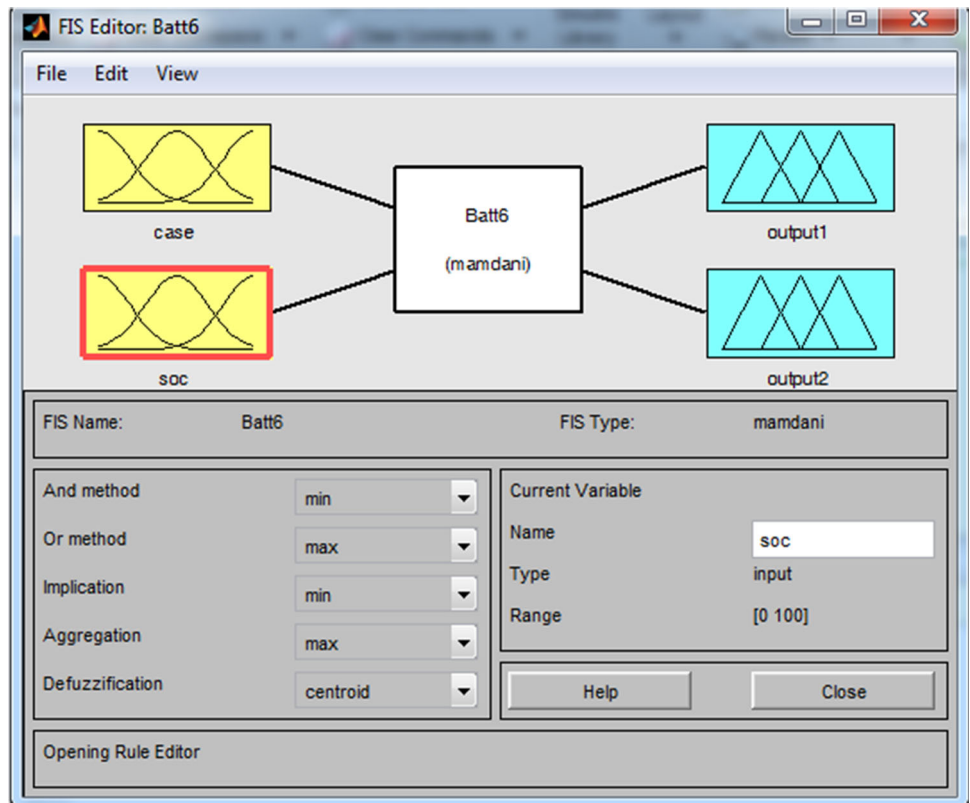
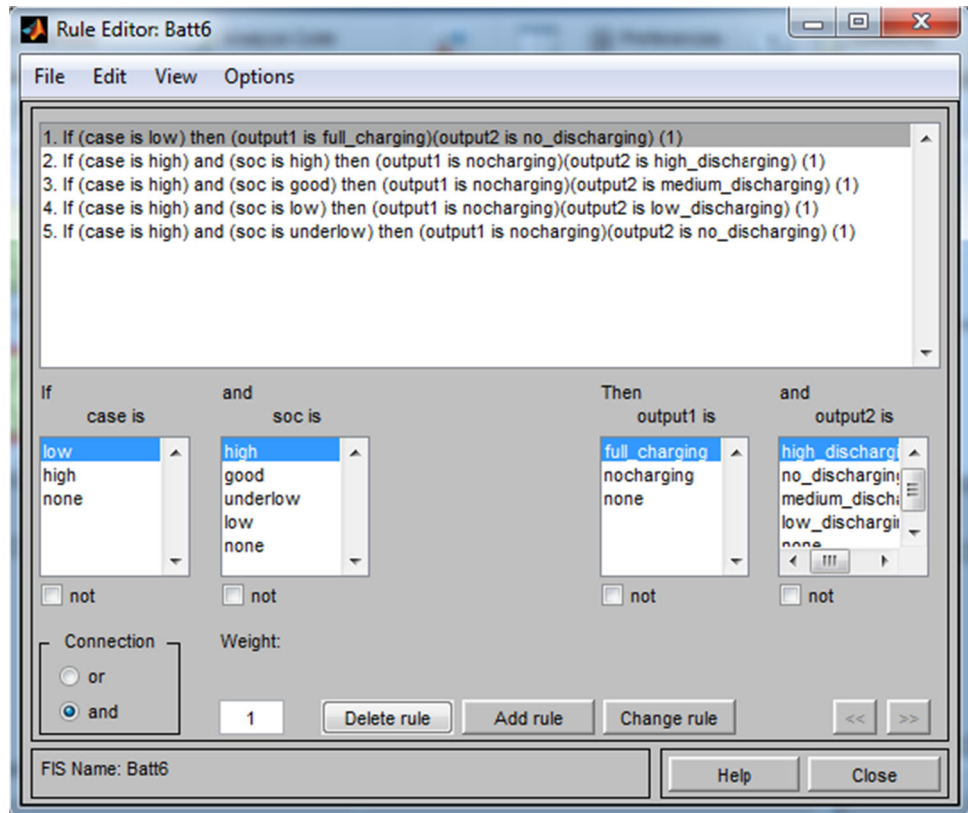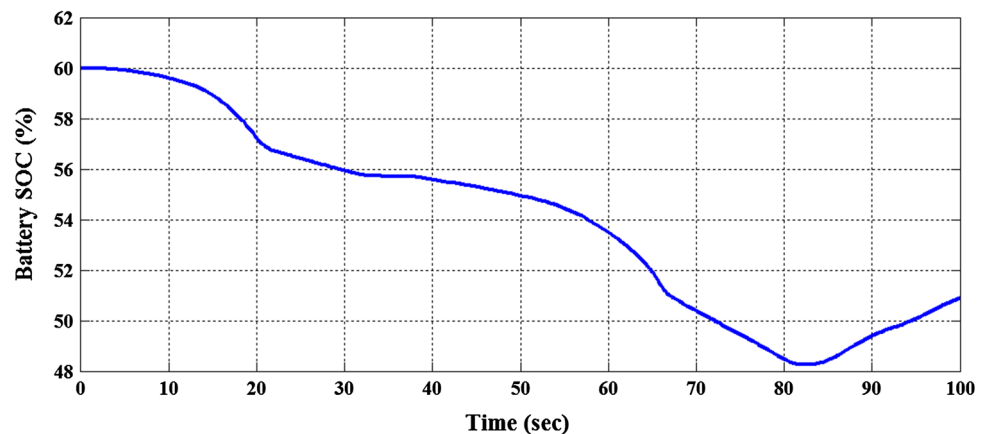**Fig. 29** Hydrogen mass in the fuel tank
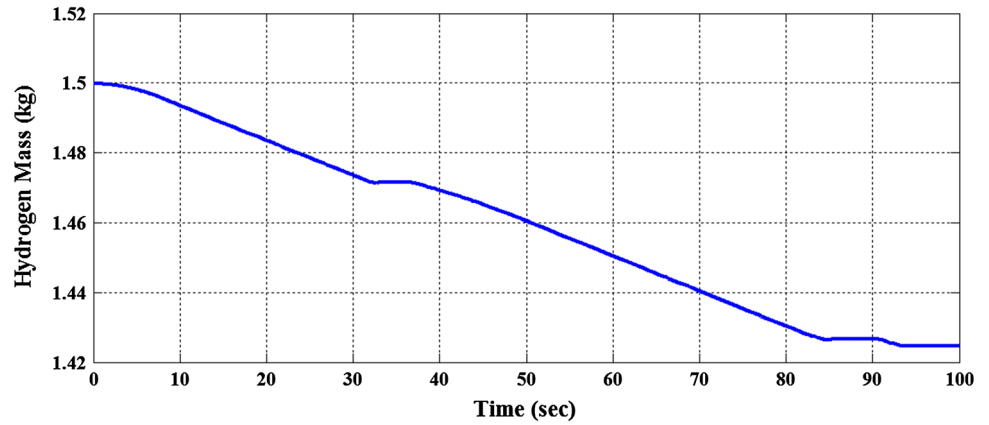
Fig. 30 Battery SOC variations by employing controller #1
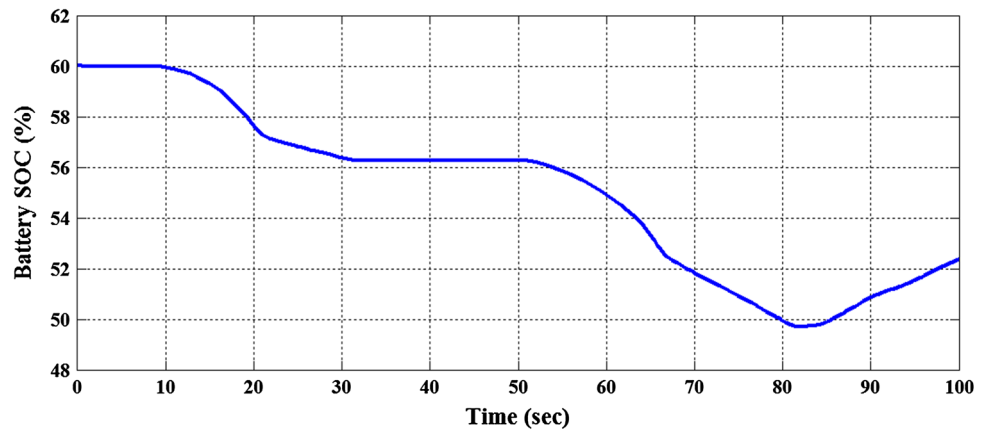
Fig. 31 Schematic of fuzzy interface system (FIS) designed in Matlab fuzzy toolbox

390

J Braz. Soc. Mech. Sci. Eng. (2015) 37:375–396

Fig. 32 Rule sets in FIS design

Fig. 33 Battery SOC variations by employing controller #2

significantly (for instance, at the final seconds of the simulation). At the end of the simulation, without the battery charged, approximately 5 % of the fuel is consumed.

4.2 Battery state of charge control

In Sect. 4.1, battery SOC was not controlled and at the end of the simulation, battery SOC approached the restricted band and remained in that level without the battery being charged. To prevent this unfavorable case, a controller is employed.

In this section, two controllers that are separately used in the model are utilized; therefore, the simulation is performed twice with the same inputs and initial conditions and their deployment results, in terms of SOC variations and fuel consumption, will be stated.
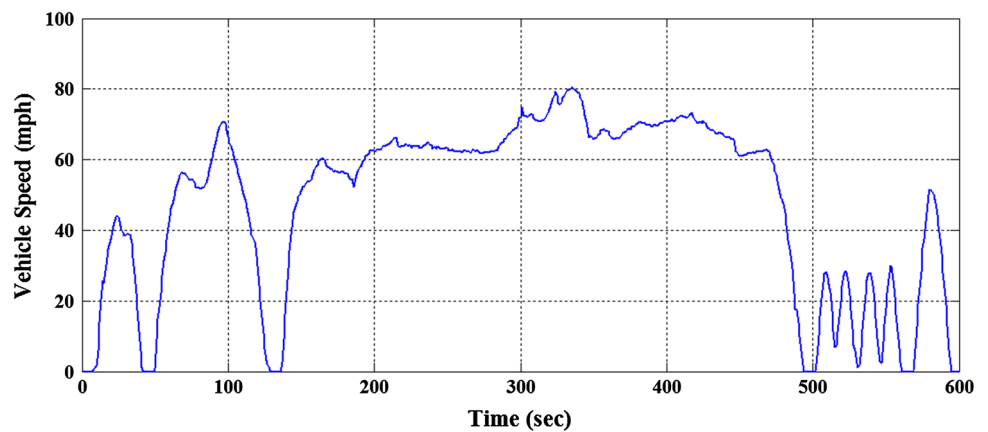
4.2.1 Controller #1

The input of this controller is battery SOC and its output is charging command with battery nominal power. This is an on–off controller and operates so that when the SOC
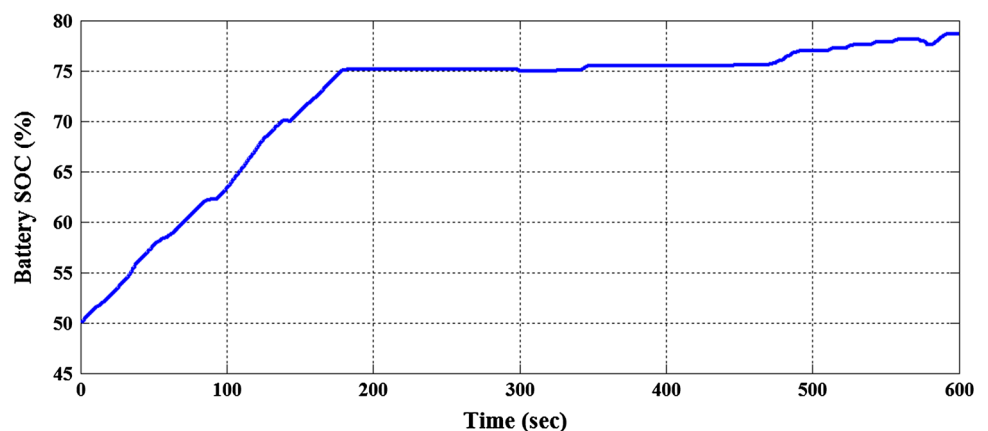
Fig. 34 Fuel consumption when employing two controllers of battery SOC
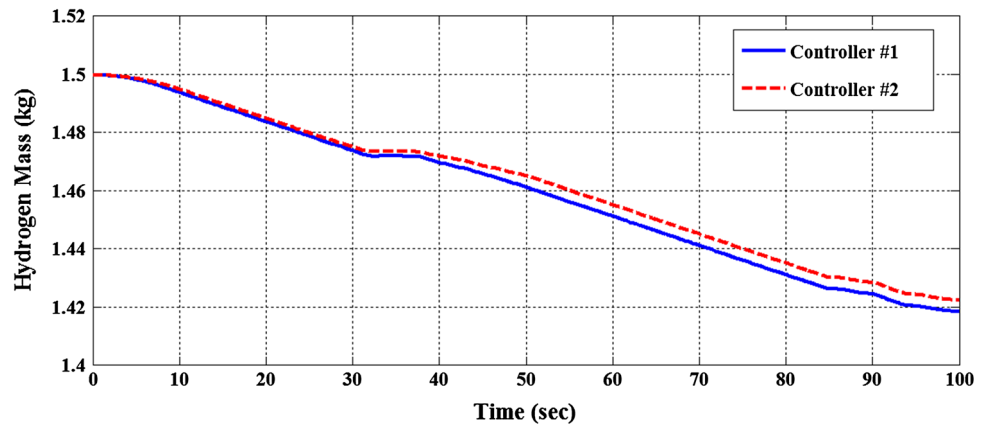
Fig. 35 US06 city driving cycle

Fig. 36 Battery SOC variations by employing controller #1 during US06 city driving cycle

reached the restricted area (50 % and below), it commands the fuel cell to charge the battery with its nominal power; in this case, fuel cell (DC–DC converter), both charges the battery and provides the power to the traction motor. When the SOC reached the desired level (75 %), battery charging stops. In this case, if fuel cell (DC–DC converter) power is less than required traction power, the battery compensates for the power shortage and when its SOC reached the restricted area, it is charged again. This type of battery SOC controller is used in Honda FCX Clarity vehicle.

In Fig. 30, simulation result using this controller is depicted. It is noted that, at almost $t = 80$ s, the SOC reaches 50 % and then the battery is charged.
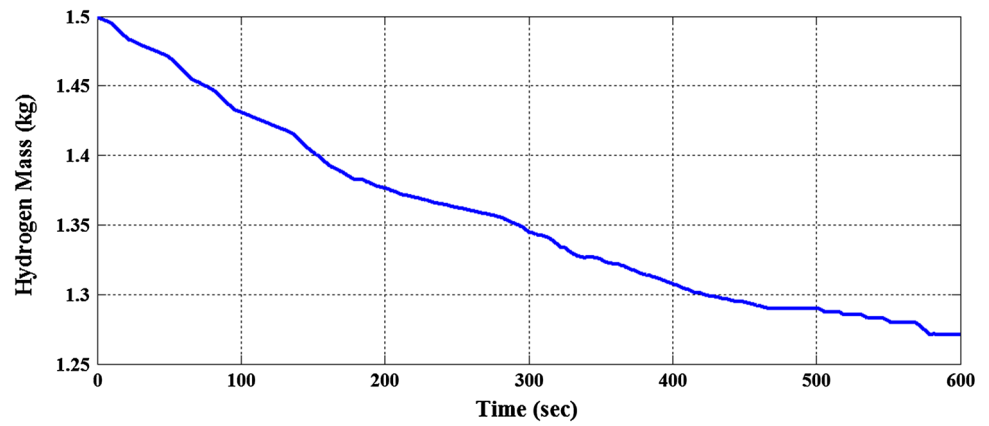
4.2.2 Controller #2

This controller is selected from fuzzy logic toolbox in Simulink software. The fuzzy interface system (FIS) is of mamdani type with triangular membership functions. The controller input is battery SOC and its output is battery
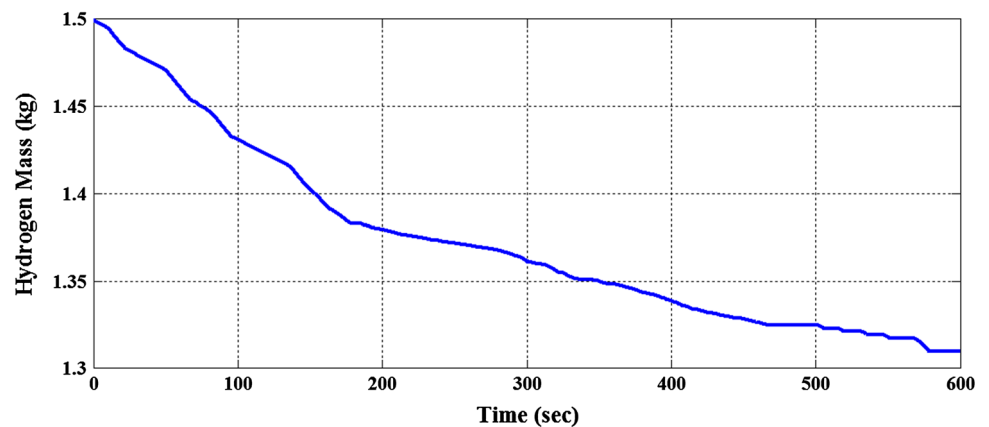
Fig. 37 Battery SOC variations by employing controller #2 during US06 city driving cycle
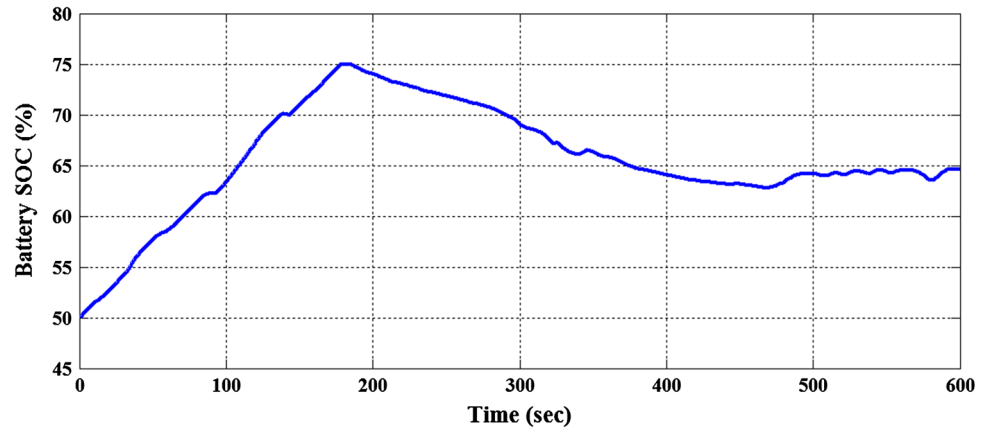
Fig. 38 Hydrogen consumption by employing controller #1 during US06 city driving cycle

Fig. 39 Hydrogen consumption by employing controller #2 during US06 city driving cycle

charge power command. The FIS system is designed in such a way that when the SOC becomes 50 %, the battery is charged, with the nominal power, to 75 %. When it reached 75 %, the controller does not command any more charging. In this case, the battery attempts to provide a proportion of the required traction power in the following manner:

- If the SOC is higher than 65 %, the battery provides 40 % of the traction power (it must be mentioned here

that the SOCs higher than 75 % are only achievable by regenerative braking);
- If the SOC is between 65 and 55 %, the battery provides 20 % of required traction power; and
- If the SOC is between 55 and 50 %, the provided power by battery is 5 % of the required traction power.

This discharging process proceeds until the SOC reaches 50 %, and as mentioned before, the battery is again charged to the desired level (75 %). The purpose of

Fig. 40 US06 highway driving cycle
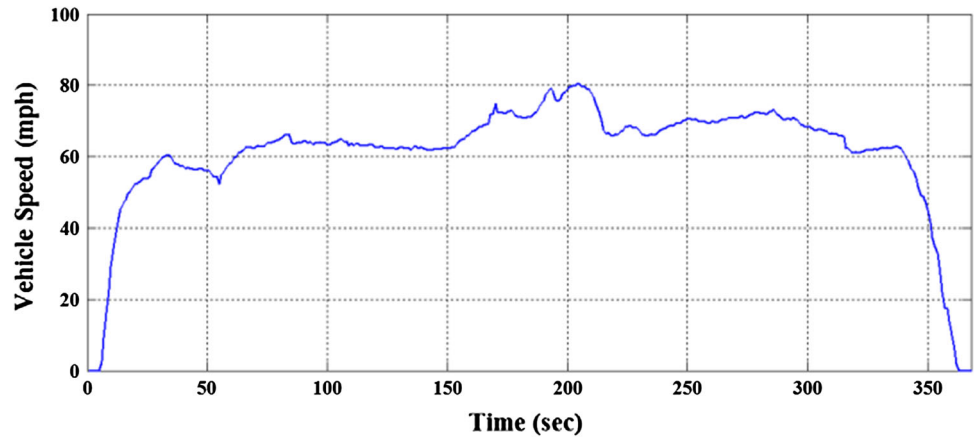
Fig. 41 Battery SOC variations by employing controller #1 during US06 highway driving cycle
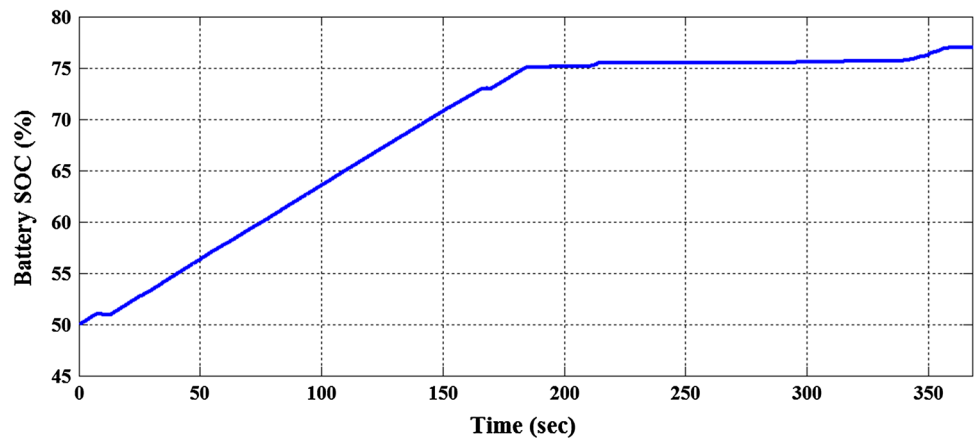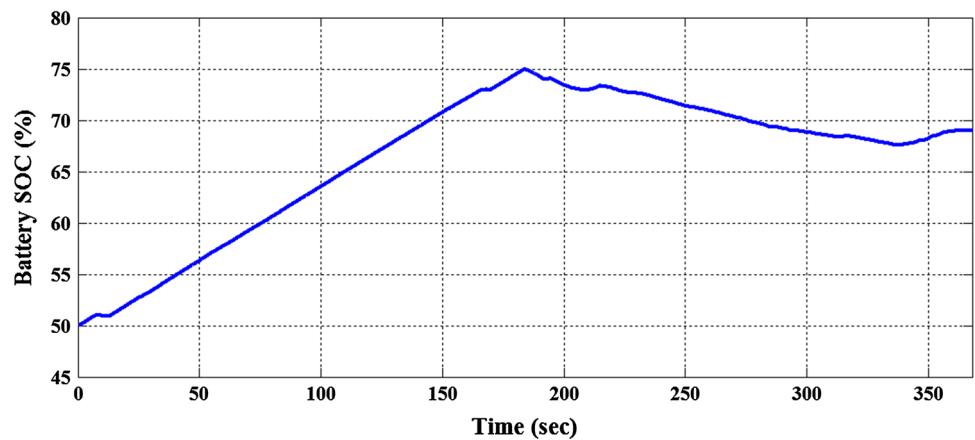

Fig. 42 Battery SOC variations by employing controller #2 during US06 highway driving cycle

designing this controller is that the battery, while having sufficient SOC, supports the fuel cell and contributes to providing required traction power (Figs. 31, 32).

Figure 33 shows the simulation result of using this controller.

It is noticed that between $t = 70$ and 80 s, the SOC drops under 50 % and after $t = 80$ s the battery is charged. This happening can be justified by the current drawn from fuel cell in Fig. 26. In this figure, it is seen that almost until $t = 83$ s, the drawn current from fuel cell is maximum (due to vehicle speed and road slope). This situation in driving cycle also existed for controller #1, but since using controller #2, the battery assists the fuel cell in providing traction power, the SOC, at any instant, is lower than the case of using controller #1; therefore, this drop in SOC can be justified. Controller #2 tends to discharge the battery in

394

J Braz. Soc. Mech. Sci. Eng. (2015) 37:375–396

Fig. 43 Hydrogen consumption by employing controller #1 during US06 highway driving cycle

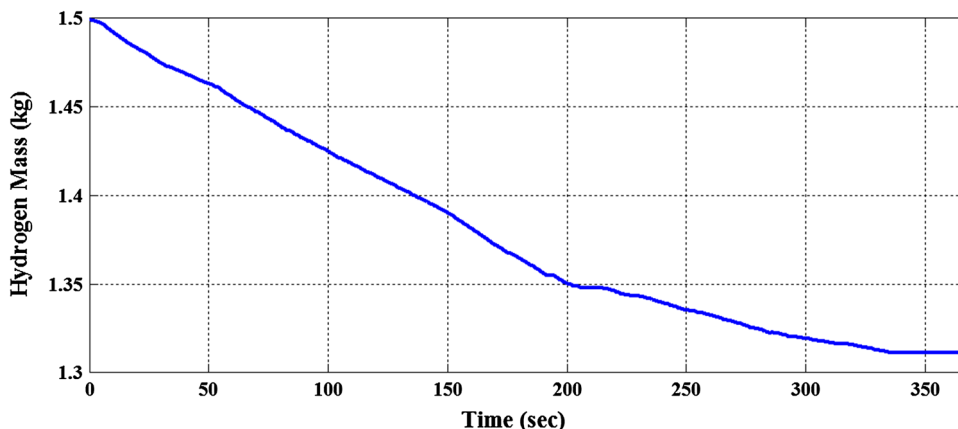**Fig. 44** Hydrogen consumption by employing controller #2 during US06 highway driving cycle
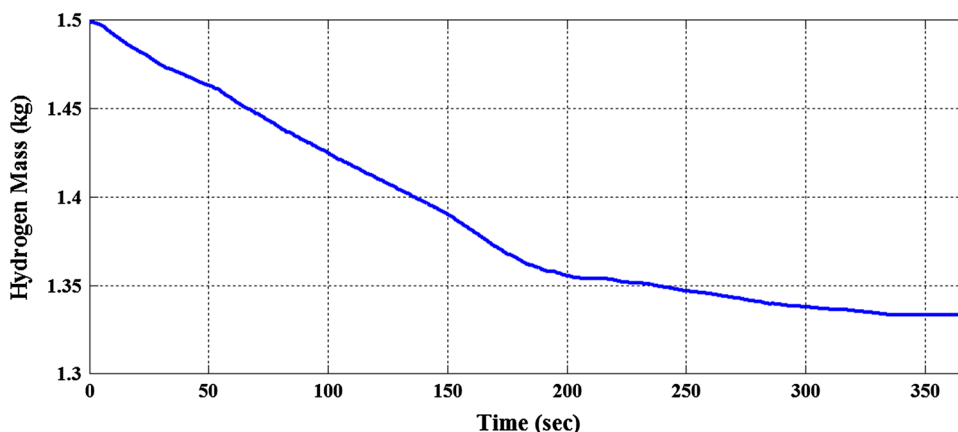
Table 2 Fuel consumption comparison during two driving cycles with the two battery SOC controllers

	Hydrogen consumption percentage during US06 city driving cycle	Hydrogen consumption percentage during US06 highway driving cycle
Controller #1	15.3	12.6
Controller #2	12.7	11.1

this simulation (with initial SOC of 60 %), while with controller #1 the battery is discharged only when the fuel cell current is maximum and fuel cell fails to provide more power for traction. It is seen in Fig. 33 that the battery is charged after the current drawn from fuel cell goes less than the maximum amount.

Figure 34 illustrates vehicle fuel consumption using these two controllers. It can be noticed that by employing controller #2, less fuel is consumed.

4.3 Vehicle performance simulation during driving cycle

In this section, two driving cycles are used as input to investigate vehicle performance in terms of battery SOC and hydrogen consumption. These cycles are US06 city and US06 highway and are chosen from Advisor software.

The road slope input, in fuel cell vehicle model, is selected to be zero. Initial hydrogen mass is again assumed to be 1.5 kg. The initial SOC is selected 49.9 % so that the performance of controllers is better studied.

Figure 35 shows vehicle speed in US06 city driving cycle and Figs. 36, 37, 38, 39 illustrate battery SOC variations and hydrogen consumption with controllers #1 and #2 during this cycle.

In figures above, it is obvious that the fuel cell hybrid vehicle consumes less hydrogen by employing controller #2. This can be accounted for by the fact that with controller #1, first the battery is charged to the desired level and then is discharged only when the fuel cell current exceeds the maximum allowable current and the traction motor requires more power than the power provided by fuel cell. In this condition, battery is discharged to compensate for power shortage; but using controller #2, the battery is first charged to the desired level and then is discharged; hence, fuel current decreases and as a result hydrogen consumption reduces.

Figure 40 displays vehicle speed during US06 highway driving cycle.

Figures 41, 42, 43, 44 illustrate battery SOC variations and hydrogen consumption with controllers #1 and #2 during this cycle.

It is clear that fuel consumption using controller #2 is less than the one with controller #1.

In Table 2, the results in terms of fuel consumption percentage, during these two driving cycles and with the two controllers are shown.

5 Conclusions

In this paper, a FC hybrid vehicle model was proposed and simulated in Matlab/Simulink environment. Fuel cell system was modeled and simulated in an earlier publication by the authors. It is comprised of: cathode air supply system model, anode hydrogen supply system model, fuel cell stack model, water and heat management models. In this model, water management system is not considered and is assumed to be well controlled and the system is maintained in our desired conditions. Other elements in the vehicle which are modeled and simulated are: DC–DC converter, electric motor, transmission and vehicle. The electric motor has the capability of energy storage from regenerative braking. A model for Li-ion battery, as the auxiliary power source, is proposed in this paper, but a model of Simulink software is used.

Subsequently, using a static controller, the fuel cell power system is set to function with its maximum efficiency. Stack temperature is also controlled by a PID controller. The results suggest that these controllers work well and satisfactory performance of the system is guaranteed. Fuel cell polarization curve and system efficiency versus current density are obtained. The outcomes of these two curves suggest that current density must not exceed the value of 0.9 to prevent system losses. Considering this fuel cell specifications, it is concluded that fuel cell current must have a maximum limit of 252 amp. Following that, the proposed FC model is adapted for a Nexa fuel cell power module and simulation results are validated with experimental results leading to satisfactory outcomes.

Finally, the whole fuel cell hybrid vehicle is simulated. Traction motor required power, fuel cell current and terminal voltage, DC–DC converter output voltage, battery SOC and hydrogen consumption are obtained for two inputs of vehicle velocity and road slope. The results illustrate that a DC–DC converter is a vital element utilized in the circuit, which helps in avoiding large BUS voltage variations that are unfavorable for the electric traction motor. To control battery SOC, two controllers are proposed and the simulation results are acquired for each of them that are separately used. These results approve that each of two controllers is capable of keeping the SOC out of the restricted band; but controller #2 (a fuzzy controller) makes the fuel cell consume less hydrogen. Following that, to obtain comparable results, the performance of these two controllers is tested during two driving cycles. Controller #2 again proves to be capable of reducing vehicle fuel consumption during both cycles and this can be justified by this fact that the less current is drawn from fuel cell, the less hydrogen is consumed. Controller #2 is designed to benefit from this fact. Here, the battery makes vehicle performance and hydrogen consumption improve; a fact that could be predicted beforehand.

References

1. Rajashekara K (2000) Propulsion system strategies for FC vehicles. SAE Paper, 2000-01-0369
2. Thring RH (2004) Fuel cells for automotive applications. Professional Engineering, Baltimore
3. Shan Y, Choe SY (2005) A high dynamic PEM FC model with temperature effects. J Power Sour 145:30
4. Pukrushpan JT, Stefanopoulou AG, Peng H (2004) Control of FC breathing. IEEE Control Syst Mag 24(2):30–46
5. Pukrushpan J, Stefanopoulou AG, Peng H (2005) Control of FC power systems. Springer, London
6. Schell A, Peng H, Tran D, Stamos E, Lin ChCh, Kim MJ (2005) Modeling and control strategy development for FC electric vehicles. Annu Rev Control 29:159
7. Sharifi Asl SM, Rowshanzamir S, Eikani MH (2010) Modelling and simulation of the steady-state and dynamic behaviour of a PEM fuel cell. Energy 35:1633–1646
8. Moore RM, Hauer KH, Friedman D, Cunningham J, Badrinarayanan P, Ramaswamy S, Eggert A (2005) A dynamic simulation tool for hydrogen FC vehicles. J Power Sour 141:272–285
9. Ehsani M, Gao Y, Emadi A (2010) Modern electric, hybrid electric, and fuel cell vehicles: fundamentals, theory, and design, 2nd edn. CRC Press-Taylor & Francis Group, Boca Raton
10. Halderman JD, Martin T (2009) Hybrid and alternative fuel vehicles. Pearson-Prentice Hall, NJ
11. Hosseini SM, Shamekhi AH, Yazdani A (2012) Dynamic modelling and simulation of a polymer electrolyte membrane fuel cell used in vehicle considering heat transfer effects. J Renew Sustain Energy 4:043107
12. Larminie J, Dicks A (2002) FC systems explained. Wiley, New York
13. Leměs Z, Vath A, Hartkopf Th, Ancher HM (2006) Dynamic FC models and their application in hardware in the loop simulation. J Power Sour 154:386–393
14. Erdinc O, Vural B, Uzunoglu M, Ates Y (2009) Modeling and analysis of an FC/UC hybrid vehicular power system using a wavelet-fuzzy logic based load sharing and control algorithm. Int J Hydrogen Energy 34:5223–5233
15. Chiu LY, Diong BM (2004) An improved small-signal model of the dynamic behavior of PEM fuel cells. IEEE Trans Ind Appl 40:970–977
16. Gou B, Na WK, Diong B (2010) Fuel cells: modeling, control, and applications. CRC Press-Taylor & Francis Group, Boca Raton
17. Fuhs AE (2009) Hybrid vehicles and the future of personal transportation. CRC Press-Taylor & Francis Group, Boca Raton

18. Vahidi A, Stefanopoulou A, Peng H (2006) Current management in a hybrid fuel cell power system: a model predictive control approach. Department of Mechanical Engineering, University of Michigan

19. Arce A, del Real AJ, Bordons C (2009) MPC for battery/fuel cell hybrid vehicles including fuel cell dynamics and battery performance improvement. J Process Control 19:1289–1304

20. Lechner G, Naunheimer H (1999) Automotive transmissions: fundamentals, selection, design and application. Springer, Berlin

21. Soltani M, Mohammad Taghi Bathaee S (2010) Development of an empirical dynamic model for a Nexa PEM fuel cell power module. Energy Convers Manag 51:2492–2500